Electron Scavenging by Conductive Nanoparticles in Oil Insulated Power Transformers

J. George Hwang, *Student Member, IEEE,* Markus Zahn, *Fellow, IEEE,* Francis M. O'Sullivan, Leif A. A. Pettersson, Olof Hjortstam, and Rongsheng Liu, *Senior Member, IEEE*

(Invited Paper)

***Abstract*—Transformer oil-based nanofluids with conductive nanoparticle suspensions have been experimentally shown to have substantially higher positive voltage breakdown levels with slower positive streamer velocities than that of pure transformer oil. A comprehensive electrodynamic analysis of the processes which take place in electrically stressed transformer oil-based nanofluids has been developed and a model is presented for streamer formation in transformer oil-based nanofluids. Through the use of numerical simulation methods the model demonstrates that conductive nanoparticles act as electron scavengers in electrically stressed transformer oil-based nanofluids converting fast electrons to slow negatively charged particles. Due to the low mobility of these nanoparticles the development of a net space charge zone at the streamer tip is hindered suppressing the propagating electric field wave that is needed to continue electric field dependent molecular ionization and ultimately streamer propagation further into the liquid. General expressions for the charging dynamics of a nanoparticle in transformer oil with both infinite and finite conductivities are derived to show that the trapping of fast electrons onto slow conducting nanoparticles is the cause of the decrease in positive streamer velocity and higher electrical breakdown strength.**

***Index Terms*—Electrical breakdown, field ionization, nanofluid, nanoparticle, streamers, transformer oil.**

I. Introduction

THE widespread use of transformer oil for high voltage insulation and power apparatus cooling has led to extensive research work aimed at enhancing both its dielectric and thermal characteristics. A particularly innovative example of such work is the development of dielectric nanofluids. These materials are manufactured by adding nanoparticle suspensions to transformer oil, with the aim of enhancing some of the oil's insulating and thermal characteristics. Segal *et al.* investigated transformer oil-based nanofluids, using magnetite nanoparticles [1]–[3]. The research aimed to explore if a transformer oil-based magnetic nanofluid could be used to enhance the cooling of a power transformer's core.

J. G. Hwang and M. Zahn are with the Department of Electrical Engineering and Computer Science, Laboratory for Electromagnetic and Electronic Systems, Massachusetts Institute of Technology, Cambridge, MA, 02139 USA e-mail: ghwang@mit.edu, zahn@mit.edu.

F. M. O'Sullivan is with the MIT Energy Initiative, Massachusetts Institute of Technology, Cambridge, MA, 02139 USA e-mail: frankie@mit.edu.

L. A. A. Pettersson and R. Liu are with ABB Corporate Research, Power Technologies, S-72178 Västerås, Sweden e-mail: leif.a.pettersson@se.abb.com, rongsheng.liu@se.abb.com.

O. Hjortstam is with ABB AB, Metallurgy, S-72159 Västerås, Sweden e-mail: olof.hjortstam@se.abb.com.

Manuscript received April 17, 2009.

Electrical breakdown testing of magnetite nanofluid found that for positive streamers the breakdown voltage of the nanofluids was almost twice that of the base oils during lightning impulse tests. The lightning impulse withstand results obtained by Segal *et al.* for two common transformer oils (*i.e.*, Univolt 60 and Nytro 10X) and their associated nanofluids are summarized in Table I. Also, the propagation velocity of positive streamers was reduced by the presence of nanoparticles, by as low as 46% for Univolt-Colloid Nanofluid. The results are significant because a slower streamer requires more time to traverse the gap between electrodes to cause breakdown. This allows more time for the applied impulse voltage to be extinguished. These results are very important in that it indicates that the presence of the magnetite nanoparticles in the oil samples inhibits the processes which lead to electrical breakdown. The results found by Segal *et al.* are in direct conflict with conventional wisdom regarding the breakdown of dielectric liquids, which suggests that the presence of conducting particulate matter in a dielectric liquid will decrease the breakdown strength.

A comprehensive electrodynamic analysis of the processes that take place in electrically stressed transformer oil-based nanofluids has been developed. The results demonstrate that conductive nanoparticles act as electron scavengers in electrically stressed transformer oil-based nanofluids converting fast electrons to slow charged particles [4], [5]. Due to the low mobility of these nanoparticles the development of a net space charge zone at the streamer tip is hindered, suppressing the propagating electric field wave that is needed to drive electric field dependent molecular ionization and ultimately streamer propagation further into the liquid. A general expression for the charging dynamics of a nanoparticle in transformer oil with finite conductivity is derived to show that the trapping of fast electrons onto slow nanoparticles is the cause of the decrease in positive streamer velocity. This explains the paradoxical fact that nanofluids manufactured from conductive nanoparticles have superior positive electrical breakdown performance to that of pure oil.

An electrodynamic model is presented for streamer formation in transformer oil-based nanofluids. The model is analyzed numerically via the finite element simulation package COMSOL Multiphysics. This study builds upon earlier work that showed that transformer oil stressed by a positively charged electrode leads to molecular ionization of oil molecules into slow positive ions and fast electrons [4], [5]. The fast electrons cause a propagating electric field wave that is the dominant

TABLE I
RESULTS OF IMPULSE VOLTAGE WITHSTAND TESTING IN 25.4 MM ELECTRODE GAP SYSTEM [2]

Fluid	**Breakdown Voltage**		**Time to Breakdown**		**Average Streamer Velocity**	
	Positive	Negative	Positive	Negative	Positive	Negative
Univolt 60 Transformer Oil	86 kV	170 kV	12 μs	27 μs	2.12 km/s	0.94 km/s
Univolt-Colloid Nanofluid	157 kV	154 kV	26 μs	15 μs	0.98 km/s	1.69 km/s
Nytro 10X Transformer Oil	88 kV	177 kV	16 μs	23 μs	1.59 km/s	1.10 km/s
Nytro-Colloid Nanofluid	156 kV	173 kV	25 μs	17 μs	1.02 km/s	1.49 km/s

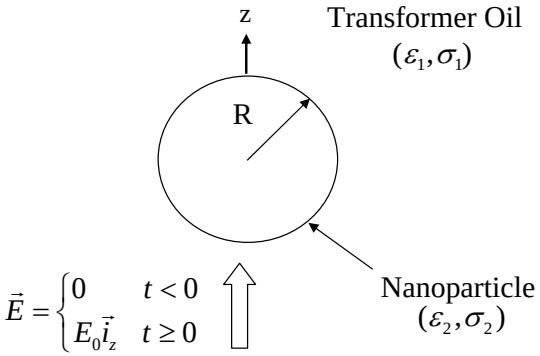

Fig. 1. Nanoparticle of an arbitrary material with a radius R, permittivity ϵ_2 and conductivity σ_2, surrounded by transformer oil with a permittivity of ϵ_1 and conductivity σ_1 stressed by a uniform z-directed electric field turned on at $t = 0$.

mechanism in streamer propagation leading to electrical breakdown.

II. NANOPARTICLE RELAXATION TIMES

To understand why a transformer oil-based nanofluid exhibits differing electrical breakdown characteristics to that of pure oil, it is necessary to understand how the presence of the nanoparticles in the oil modifies the fundamental electrodynamic processes. The charge relaxation time constant of the nanoparticle material has a major bearing on the extent to which the electrodynamic processes in the liquid are modified. If the nanoparticles' charge relaxation time constant is short relative to the timescales of interest for streamer growth, their presence in the oil will significantly modify the electrodynamics. If on the other hand the nanoparticles' relaxation time constant is long relative to the timescales of interest for streamer growth, their presence will have little effect upon the electrodynamics.

In order to calculate a general expression for the relaxation time constant of a nanoparticle of arbitrary material in transformer oil consider Fig. 1. The spherical nanoparticle of an arbitrary material has radius R, permittivity ϵ_2 and conductivity σ_2, and is surrounded by transformer oil with conductivity $\sigma_1 = 1 \times 10^{-12}$ S/m and permittivity $\epsilon_1 = 2.2\epsilon_0$ where $\epsilon_0 = 8.854 \times 10^{-12}$ F/m is the permittivity of free space. At time $t = 0^+$ a z-directed electric field $\vec{E} = E_0 \vec{i}_z$ is switched on at $r \to \infty$. The presence of the nanoparticle causes the electric field distribution in the oil near the nanoparticle to deviate from the applied z-directed field. The electric field distribution in the oil is calculated by using the separation of variables method to solve Laplace's equation (*i.e.*, $\nabla^2 V = 0,\ \vec{E} = -\nabla V$) where a negligible space charge density is assumed. The time dependent radial and polar components of the electric field in the oil outside of the nanoparticle are [4], [6], [7]

$$E_{r0}(r,\theta) = E_0 \left[1 + \frac{2R^3}{r^3} \Upsilon_c \exp\left(-\frac{t}{\tau_r}\right) + \frac{2R^3}{r^3} \Sigma_c \left(1 - \exp\left(-\frac{t}{\tau_r}\right)\right) \right] \cos\theta \tag{1}$$

$$E_{\theta 0}(r,\theta) = E_0 \left[-1 + \frac{R^3}{r^3} \Upsilon_c \exp\left(-\frac{t}{\tau_r}\right) + \frac{R^3}{r^3} \Sigma_c \left(1 - \exp\left(-\frac{t}{\tau_r}\right)\right) \right] \sin\theta \tag{2}$$

where the charge relaxation time constant τ_r for the transformer oil/nanoparticle system is

$$\tau_r = \frac{2\epsilon_1 + \epsilon_2}{2\sigma_1 + \sigma_2} \tag{3}$$

and

$$\Upsilon_c = \frac{\epsilon_2 - \epsilon_1}{2\epsilon_1 + \epsilon_2} \tag{4}$$

$$\Sigma_c = \frac{\sigma_2 - \sigma_1}{2\sigma_1 + \sigma_2}\ . \tag{5}$$

Consider now the magnetite (Fe_3O_4) nanofluid studied by Segal *et al.* in [2] where $\sigma_2 = 1 \times 10^4$ S/m at room temperature [8], and $\epsilon_2 \approx 80\epsilon_0$ [9]. The relaxation time constant of magnetite in transformer oil is $\tau_{r(Fe_3O_4)} = 7.5 \times 10^{-14}$ s. As this shows, the relaxation time constant for magnetite nanoparticles in transformer oil is extremely short. Relative to the nanosecond to microsecond timescales involved in streamer propagation, this small relaxation time constant is essentially instantaneous so that the addition of magnetite nanoparticles to the transformer oil will dramatically affect the electrodynamics during streamer development. The relaxation time constant is analogous to the time constant of an RC circuit that describes the charging rate of a capacitor (nanoparticle) when the source (free electrons at $r \to \infty$) is turned on at $t = 0$. Therefore, the small time constant for magnetite nanoparticles effectively means that the surface charging due to the injected electrons can be considered to be instantaneous. Furthermore, for a nanofluid manufactured using magnetite, the extremely short relaxation time constant means that the electric field lines

tend to converge upon the relaxed nanoparticles as if they were perfect conductors.

As a comparison to the nanofluid manufactured with magnetite nanoparticles, other common nanoparticles such as ZnO ($\sigma_2 = 10$ S/m, $\epsilon_2 = 7.4\epsilon_0$) and Al_2O_3 ($\sigma_2 = 1 \times 10^{-12}$ S/m, $\epsilon_2 = 9.9\epsilon_0$) have relaxation time constants of $\tau_{r(\mathrm{ZnO})} = 1.045 \times 10^{-11}$ s and $\tau_{r(\mathrm{Al_2O_3})} = 42.2$ s. Note that due to Al_2O_3's low conductivity, its relaxation time constant is very long. Therefore, there would be negligible surface charging of Al_2O_3 nanoparticles in the microsecond timescales of interest for which streamer development occurs.

III. Modeling the Charging Dynamics of a Nanoparticle

To model the electrodynamics within an electrically stressed transformer oil-based nanofluid it is first necessary to model the charging of the nanoparticles in oil. This model parallels the Whipple-Chalmers model used for the modeling of rain drop charging in thunderstorms taking the flow velocity of oil to be zero [6], [7], [10]. Consider the situation shown in Fig. 2 for the nanoparticle with conductivity σ_2 and permittivity ϵ_2. A uniform z-directed electric field $E_0\vec{i}_z$ is switched on at $t = 0$, and a uniform electron charge density ρ_e due to ionization and electron mobility μ_e is injected into the system from $z \to \infty$. The injected electrons travel along the electric field lines and approach the nanoparticle where the radial electric field is positive, $0 < \theta < \pi/2$. Once a nanoparticle has relaxed electrically, the electric field lines will terminate on the bottom side with a negative surface charge and emanate from the top side positive surface charge of the particle as shown in Fig. 2(a). The electrons present in the transformer oil in the vicinity of any given nanoparticle will move opposite to the direction of the field lines and become deposited on the nanoparticle where the surface charge is positive. The rate at which a nanoparticle captures electrons is strongly dependent upon its relaxation time constant such that nanoparticles with a short relaxation time constant quickly capture free electrons.

The charging dynamics for a perfectly conducting nanoparticle ($\sigma_2 \to \infty$) is examined first. Afterwards, the analysis is generalized to finitely conducting nanoparticles to model nanoparticles manufactured from real materials.

A. Perfectly Conducting Nanoparticle

At $t = 0^+$, a nanoparticle with infinite conductivity is perfectly polarized and the radial electric field is positive everywhere on the upper hemisphere defined by $\theta = 0$ to $\pi/2$ as shown in Fig. 2(a). Therefore, the electrons can be deposited on the particle at all points on the upper hemispherical surface. Once the electrons deposit on the particle they redistribute themselves uniformly on the equipotential surface, so that the total negative charge on the nanoparticle increases with time. This charging process modifies the electric field outside the nanoparticle and continually reduces the area of the nanoparticle surface that has a positive radial electric field component (the charging window on the particle surface) as shown in Fig. 2(b) until a point is reached when no portion of the particle's surface has a positive radial electric field component as shown in Fig. 2(c). In this situation the nanoparticle is said

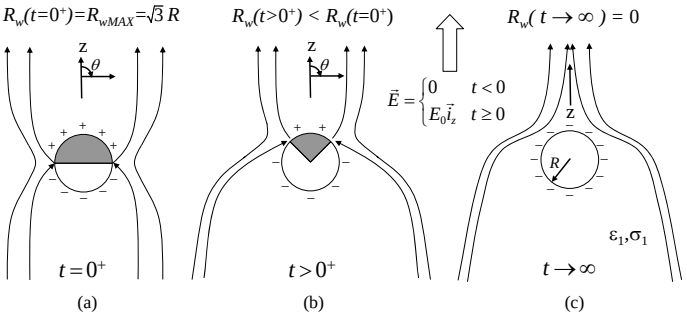

Fig. 2. Nanoparticle of a perfectly conducting material with a radius R surrounded by transformer oil with a permittivity of ϵ_1 and conductivity σ_1 stressed by a uniform z-directed electric field. (a) At time $t = 0^+$ the nanoparticle is polarized and all the electric field lines which pass through the cross sectional area of radius $\sqrt{3}R$ will terminate on the nanoparticle such that the electron charging window is at a maximum, $R_w(t = 0^+) = R_{wMAX} = \sqrt{3}R$. The nanoparticle is polarized with positive surface charge for $0 < \theta < \pi/2$ and negative surface charge for $\pi/2 < \theta < \pi$. (b) At later times $t > 0^+$, the electron charge deposited on the particle modifies the surrounding electric field distribution and the charging window is $0 < R_w(t) < R_{wMAX}$ where $R_w(t)$ is the cylindrical radius given in (27). (c) As $t \to \infty$, the electric field distribution is modified until a point where no field lines terminate on the particle and $R_w(t \to \infty) = 0$. In this situation, a perfectly conducting nanoparticle is fully charged with a total charge of $Q_s = -12\pi\epsilon_1 R^2 E_0$.

to be charge saturated as no additional negative charge can flow onto the sphere.

The steady-state solution for the electric field outside the perfectly conducting (*i.e.,* $\sigma_2 \to \infty$, $\Sigma_c = 1$) spherical nanoparticle is the superposition of the steady-state solutions of (1) and (2) plus the radial field component caused by the already deposited electrons with net charge $Q(t)$ where $Q(t) \leq 0$.

$$\vec{E} = \left[E_0\left(1 + \frac{2R^3}{r^3}\right)\cos\theta + \frac{Q(t)}{4\pi\epsilon_1 r^2}\right]\vec{i}_r - E_0\left[1 - \frac{R^3}{r^3}\right]\sin\theta\ \ \vec{i}_\theta\ . \qquad r > R \tag{6}$$

Electrons can only be deposited on the nanoparticle where the radial component of the electric field on the nanoparticle surface is positive (*i.e.,* $E_r(r = R) \geq 0$). This gives a window for electron charging over a range of angles determined by

$$\cos\theta \geq -\frac{Q(t)}{12\pi\epsilon_1 E_0 R^2}\ . \tag{7}$$

Since the magnitude of $\cos\theta$ cannot be greater than one, the electron saturation charge for the nanoparticle is

$$Q_s = -12\pi\epsilon_1 R^2 E_0\ . \tag{8}$$

When the nanoparticle charges to this saturation value the radial component of the electric field at every point on the particle's surface will be negative and so no more electrons can be deposited on the particle. The critical angle θ_c, where the radial component of the electric field at $r = R$ is zero, is defined as when (7) is an equality

$$\cos\theta_c = Q(t)/Q_s\ . \tag{9}$$

The current density charging of the nanoparticle for angles $0 < \theta < \theta_c$ is

$$J_r(r = R, \theta) = -\rho_e\mu_e E_r(r = R, \theta) = -3\rho_e\mu_e E_0\left[\cos\theta - \frac{Q(t)}{Q_s}\right] \tag{10}$$

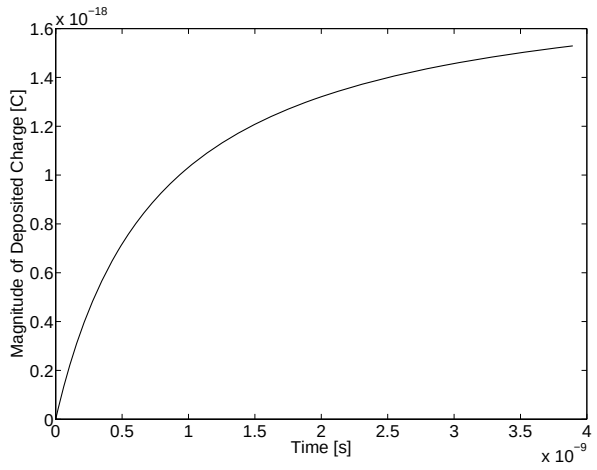

Fig. 3. Charging dynamics, $Q(t)$, of a perfectly conducting nanoparticle versus time in transformer oil as given in (13) with $Q_s = -1.836\times10^{-18}$ C and $\tau_{pc} = 7.79\times10^{-10}$ s.

where $\rho_e < 0$ and $\mu_e > 0$. The total nanoparticle charging current is

$$\frac{dQ(t)}{dt} = -\int_{\theta=0}^{\theta_c} J_r 2\pi R^2 \sin\theta d\theta = \frac{Q_s}{\tau_{pc}}\left[\frac{Q(t)}{Q_s} - 1\right]^2 \tag{11}$$

where τ_{pc} is

$$\tau_{pc} = \frac{4\epsilon_1}{|\rho_e|\mu_e} \ . \tag{12}$$

The charging dynamics of the perfectly conducting nanoparticle can be found by time integrating the nanoparticle charging current equation given by (11). Therefore, the charge on a perfectly conductive nanoparticle by electron scavenging is

$$Q(t) = \frac{Q_s \frac{t}{\tau_{pc}}}{1 + \frac{t}{\tau_{pc}}} \tag{13}$$

where the initial condition is $Q(t=0) = 0$.

For the purposes of evaluating the values of Q_s and τ_{pc}, the following parameter values are used: $e = 1.6\times10^{-19}$ C, $E_0 = 1\times10^8$ V/m, $\rho_e = -1\times10^3$ C/m^3, $\mu_e = 1\times10^{-4}$ m^2/V·s [12], [13], $\epsilon_1 = 2.2\epsilon_0$ and $R = 5\times10^{-9}$ m. These values are reasonable estimates for the parameter values at the tip of a streamer in a transformer oil-based nanofluid [5]. The values for Q_s and τ_{pc} found by using these parameters are -1.836×10^{-18} C ($\approx$ 11 electrons) and 7.79×10^{-10} s, respectively. The charging dynamics plotted in Fig. 3 illustrate that the perfectly conducting nanoparticle initially captures charge rapidly; however, as time increases the particle charging rate decreases until the particle's charge saturates at Q_s. These features are due to the reduction in the charge capture window as the particle captures electrons and the increasing repulsion between the negatively charged nanoparticle and the mobile free electrons in the surrounding oil.

Free charge carriers in the nanofluid will tend to move along the electric field lines that converge on the relaxed nanoparticle, depositing negative charge on the top surface and positive charge on the bottom surface of the particle in Fig. 2. Because electron mobility is much higher than positive ion mobility, the nanoparticles trap electrons at a much faster rate than positive ions, meaning that the nanoparticles effectively become slow negative ions. The mobility of such a charged spherical particle in transformer oil is given by (14) [7], where the viscosity of transformer oil is approximately $\eta = 0.02$ Pa·s.

$$\mu_{np} = \frac{|Q_s|}{6\pi\eta R} = 9.7\times10^{-10} \text{ m}^2/\text{V·s} \ . \tag{14}$$

B. Finitely Conducting Nanoparticle

In expanding the analysis to finitely conducting nanoparticles, it cannot be assumed that at $t = 0^+$ the nanoparticle is perfectly relaxed. Therefore, there will be some finite time, that is dependent on the particle's conductivity and permittivity, in which the nanoparticle relaxes and polarizes to the applied electric field such that in the steady state the field lines terminate and emanate perpendicular to its' surface.

Negative charge deposition on a particle takes place where the radial component of the electric field distribution on the particle surface is positive. Initially, when the particle is uncharged the radial electric field on the particle is positive for $0 < \theta < \pi/2$. However, once charge deposition occurs this situation changes and the area of the particle's surface with a positive radial field component decreases, ultimately going to zero when the particle becomes fully charged and $Q = Q_s$. As charging occurs the section of the surface that can accept charge is defined by the polar angle θ. The critical angle, θ_c, demarcates the boundary position where the radial electric field is zero. On one side of θ_c the radial electric field is positive, while on the other side the radial electric field is negative. For the perfectly conducting case illustrated in Fig. 2, at time $t = 0^+$, negative charge can be deposited at all points from $\theta = 0$ to $\pi/2$, where $\theta_C = \pi/2$. As negative charge is deposited the critical angle decreases, which corresponds with the reduction in the cylindrical radius of the charge collection window at infinity, R_w. Also, θ_c goes to 0 as $t\to\infty$, at which point the particle is fully charged and the radial electric field component is negative at every point on the particle's surface.

To develop an expression for the charging dynamics of a particle of arbitrary material in transformer oil, the effect of the deposited charge on the electric field distribution must be accounted for. The deposited charge does not affect the electric field polar component (2), however it adds a point charge-like component to the radial component of the electric field of (1) that modifies it as

$$E_r(r,\theta) = E_0\cos\theta\left[1 + \frac{2R^3}{r^3}\Upsilon_c\exp\left(-\frac{t}{\tau_r}\right) + \frac{2R^3}{r^3}\Sigma_c\left(1-\exp\left(-\frac{t}{\tau_r}\right)\right)\right] + \frac{Q(t)}{4\pi\epsilon_1 r^2} \tag{15}$$

$$E_\theta(r,\theta) = E_0\left[-1 + \frac{R^3}{r^3}\Upsilon_c\exp\left(-\frac{t}{\tau_r}\right) + \frac{R^3}{r^3}\Sigma_c\left(1-\exp\left(-\frac{t}{\tau_r}\right)\right)\right]\sin\theta \ . \tag{16}$$

As the relaxation time is non-zero, the charging angle, θ_c, has a stronger dependency on time compared to (7). Once again, electrons are deposited on the nanoparticle where $E_r(r=R,\theta)\geq 0$ and the window for electron charging over a range of angles can be determined. The critical angle, θ_c, occurs exactly at $E_r(r=R,\theta)=0$ and is

$$\cos\theta_c = \frac{3Q(t)}{Q_s A(t)} \tag{17}$$

where Q_s is the nanoparticle's electron saturation charge of (8) and

$$A(t) = 1+2\Upsilon_c \exp\left(-\frac{t}{\tau_r}\right)+2\Sigma_c\left[1-\exp\left(-\frac{t}{\tau_r}\right)\right] . \tag{18}$$

The current density charging the nanoparticle for $0<\theta<\theta_c$ is

$$\begin{aligned} J_r &= -\rho_e\mu_e E_r(r=R) \\ &= -3\rho_e\mu_e E_0\left[A(t)\cos\theta - \frac{Q(t)}{Q_s}\right] \end{aligned} \tag{19}$$

and the nanoparticle charging rate is thus

$$\begin{aligned} \frac{dQ(t)}{dt} &= -\int_{\theta=0}^{\theta_c} J_r 2\pi R^2\sin\theta d\theta \\ &= \frac{3Q_s}{\tau_{pc}A(t)}\left[\frac{Q(t)}{Q_s}-\frac{A(t)}{3}\right]^2 \end{aligned} \tag{20}$$

where Q_s, τ_{pc}, and $A(t)$ are given in equations (8), (12), and (18) respectively. Note that for a perfectly conducting particle, $\sigma_2\to\infty$, $\Sigma_c=1$, $\tau_r\to 0$, and $A(t)=3$. Then (20) reduces to (11).

C. Electric Field Lines

Analysis is also facilitated through the use of a vector potential for the electric field when the electric field due to the space charge density is small compared to the electric field due to the applied voltage so that $\nabla\cdot\vec{E}\approx 0$. Then with no dependence on the angle ϕ, $\vec{A}=A_\phi(r,\theta)\vec{i}_\phi$ and the electric field is related to the vector potential as

$$\begin{aligned} \vec{E}(r,\theta) &= \nabla\times\vec{A}(r,\theta) \\ &= \frac{1}{r\sin\theta}\frac{\partial}{\partial\theta}(\sin\theta A_\phi)\vec{i}_r - \frac{1}{r}\frac{\partial}{\partial r}(rA_\phi)\vec{i}_\theta . \end{aligned} \tag{21}$$

From (15) and (16) with (21) the vector potential is

$$\begin{aligned} A_\phi(r,\theta) = \frac{E_0 r\sin\theta}{2}\Bigg[1+\frac{2R^3}{r^3}\Upsilon_c\exp\left(-\frac{t}{\tau_r}\right) \\ +\frac{2R^3}{r^3}\Sigma_c\left(1-\exp\left(-\frac{t}{\tau_r}\right)\right)\Bigg] - \frac{Q(t)\cos\theta}{4\pi\epsilon_1 r\sin\theta} . \end{aligned} \tag{22}$$

Electric field lines are everywhere tangent to the electric field and related to the vector potential in (21) as

$$\frac{dr}{rd\theta} = \frac{E_r}{E_\theta} = \frac{\frac{1}{r\sin\theta}\frac{\partial}{\partial\theta}(\sin\theta A_\phi)}{-\frac{1}{r}\frac{\partial}{\partial r}(rA_\phi)} . \tag{23}$$

After cross multiplication and reduction, the electric field lines are lines of constant $r\sin\theta A_\phi(r,\theta)$ because

$$\frac{\partial}{\partial\theta}(r\sin\theta A_\phi)dr+\frac{\partial}{\partial\theta}(r\sin\theta A_\phi)d\theta = d(r\sin\theta A_\phi(r,\theta)) = 0 \tag{24}$$

where the constant for a given electric field line is found by specifying one (r,θ) value of a point that the field line goes through.

1) Perfectly Conducting Nanoparticle: A perfectly conducting nanoparticle has $\tau_r=0$ so that $\mathrm{e}^{-t/\tau_r}=0$, $\Sigma_c=1$, and $A(t)=3$. The field lines are obtained from (22) as

$$\begin{aligned} \Lambda_1(r,\theta) &= r\sin\theta A_\phi(r,\theta) \\ &= \frac{E_0 r^2\sin^2\theta}{2}\left[1+\frac{2R^3}{r^3}\right]-\frac{Q(t)\cos\theta}{4\pi\epsilon_1} \\ &= \text{constant} . \end{aligned} \tag{25}$$

The separation field line that demarcates the region where electrons charge a nanoparticle, as shown in Fig. 2, terminates on the nanoparticle at $r=R$, $\theta=\theta_c$ where θ_c is given in (9). This field line obeys the equation

$$\begin{aligned} \Lambda_1(r=R,\theta=\theta_c) &= \frac{3E_0R^2\sin^2\theta_c}{2}-\frac{Q(t)\cos\theta_c}{4\pi\epsilon_1} \\ &= \frac{3E_0R^2}{2}\left[1-\left(\frac{Q(t)}{Q_s}\right)^2\right]-\frac{Q^2(t)}{4\pi\epsilon_1 Q_s} . \end{aligned} \tag{26}$$

At $r\to\infty$, $\theta\to 0$ this demarcation field line has a cylindrical radius that decreases with time as the nanoparticle charges up

$$\begin{aligned} R_w(t) &= \lim_{\substack{r\to\infty\\ \theta\to 0}}(r\sin\theta) \\ &= \sqrt{3}R\left[1-\frac{Q(t)}{Q_s}\right] = \frac{\sqrt{3}R}{1+\frac{t}{\tau_{pc}}} \end{aligned} \tag{27}$$

where (13) is used.

The total current at $r\to\infty$ passing through the area $\pi R_w^2(t)$ is the total current incident onto the nanoparticle

$$\begin{aligned} I(t) &= \rho_e\mu_e E_0\pi R_w^2(t) \\ &= -3|\rho_e|\mu_e E_0\pi R^2\left[\frac{Q(t)}{Q_s}-1\right]^2 \\ &= \frac{Q_s}{\tau_{pc}}\left[\frac{Q(t)}{Q_s}-1\right]^2 \end{aligned} \tag{28}$$

which matches the right-hand side of (11).

2) Finitely Conducting Nanoparticle: Similarly, the electric field lines for a finitely conducting nanoparticle are described by (29) which is also obtained from (22). The separation field line that demarcates the region where electrons charge

$$\Lambda_2(r,\theta) = r\sin\theta A_\phi(r,\theta) = \frac{E_0 r^2\sin^2\theta}{2}\left[1+\frac{2R^3}{r^3}\Upsilon_c\exp\left(-\frac{t}{\tau_r}\right)+\frac{2R^3}{r^3}\Sigma_c\left(1-\exp\left(-\frac{t}{\tau_r}\right)\right)\right]-\frac{Q(t)\cos\theta}{4\pi\epsilon_1} = \text{constant} \tag{29}$$

a nanoparticle again terminate at $r = R,\ \theta = \theta_c$ where θ_c is given in (17)

$$\Lambda_2(r{=}R, \theta{=}\theta_c) = \frac{E_0 R^2 \sin^2\theta_c}{2} A(t) - \frac{Q(t)\cos\theta_c}{4\pi\epsilon_1} \quad (30)$$
$$= \frac{E_0 R^2}{2} A(t)\left[1 - \left(\frac{3Q(t)}{Q_s A(t)}\right)^2\right] - \frac{3Q^2(t)}{4\pi\epsilon_1 Q_s A(t)} \ .$$

At $r \to \infty$, $\theta \to 0$ this demarcation field line has a cylindrical radius of

$$R_w(t) = \lim_{\substack{r\to\infty \\ \theta\to 0}} (r\sin\theta) = \frac{3R}{\sqrt{A(t)}}\left|\frac{Q(t)}{Q_s} - \frac{A(t)}{3}\right| \ . \quad (31)$$

Note that at $t{=}0$, $Q(t{=}0) = 0$ and

$$A(t{=}0) = 1 + 2\Upsilon_c = \frac{3\epsilon_2}{2\epsilon_1 + \epsilon_2} \quad (32)$$

so that

$$R_w(t{=}0) = R\sqrt{A(t{=}0)} = R\sqrt{\frac{3\epsilon_2}{2\epsilon_1 + \epsilon_2}} \ . \quad (33)$$

If $\epsilon_2 \to \infty$ (33) reduces to $R_w(t=0) = \sqrt{3}R$ which is the same as for a perfectly conducting nanoparticle.

The total current at $r \to \infty$ passing through the area $\pi R_w^2(t)$ is the total current incident onto the nanoparticle

$$I(t) = \rho_e \mu_e E_0 \pi R_w^2(t) = \frac{3Q_s}{\tau_{pc} A(t)}\left[\frac{Q(t)}{Q_s} - \frac{A(t)}{3}\right]^2 \quad (34)$$

which matches the right-hand side of (20).

D. Evaluating Nanoparticle Charging

The solution to (20), which gives the temporal dynamics of the charge trapped on a nanoparticle in transformer oil, is not easily solved for analytically. As such, the symbolic solver from the software *Mathematica* was used to obtain the solution. A closed form solution for $Q(t)$ does exist; however, its form is exceptionally long and complicated with numerous hypergeometric functions with complex number arguments. These factors mean that it is not possible to develop an intuitive feel for the time dependent charging dynamics. A screen-shot displaying approximately 10% of the complete closed form solution for $Q(t)$ generated by *Mathematica* is shown in Fig. 4. Surprisingly, by replacing general variables with numerical values (*e.g.*, $\epsilon_1 = 2.2\epsilon_0,\ \sigma_1 = 10^{-12}$ S/m, $\epsilon_2 = \epsilon_0,\ \sigma_2 = 0.01$ S/m, $\rho_e = -10^3$ C/m^3, $\mu_e = 10^{-4}$ m^2/V·s, $\tau_r = 4.78 \times 10^{-9}$ s, $\Upsilon_c = -0.222,\ \Sigma_c = 1,\ \tau_{pc} = 7.79 \times 10^{-10}$ s), the general solution reduces to Fig. 5.

The charging dynamics of particles manufactured using materials with a range of electrical characteristics can be explored using the general solution for $Q(t)$. A number of interesting insights into the charging dynamics of particles in transformer oil can be gained from analyzing $Q(t)$ for several values of nanoparticle permittivity and conductivity. For example, in Fig. 6 three particle conductivity values ($\sigma_2 = 0.01, 0.1, 1$ S/m) and permittivity values are examined ($\epsilon_2 = \epsilon_0, 10\epsilon_0, 100\epsilon_0$) are examined. The three conductivity values are chosen to highlight the large change in nanoparticle charging dynamics for a relatively small change in conductivity (*i.e.*, poor insulator

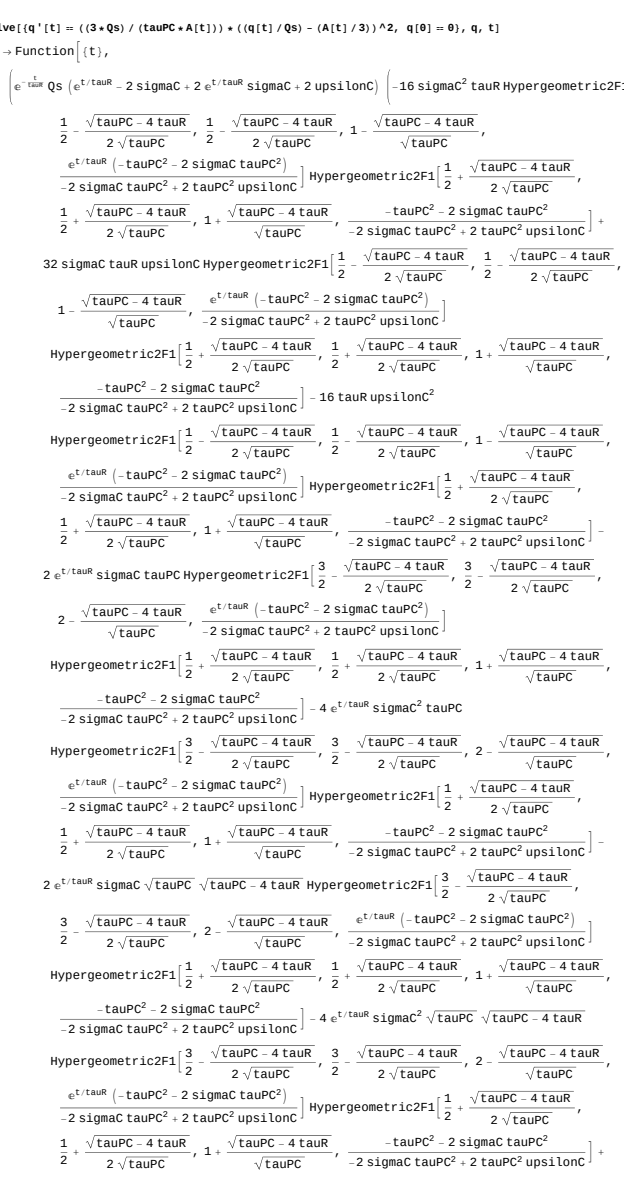

Fig. 4. Screen-shot of the initial portion of the closed form solution for $Q(t)$ in (20) generated by *Mathematica* showing the complexity of the solution with many hypergeometric functions which *Mathematica* calls `Hypergeometric2F1[a,b,c,z]` [14].

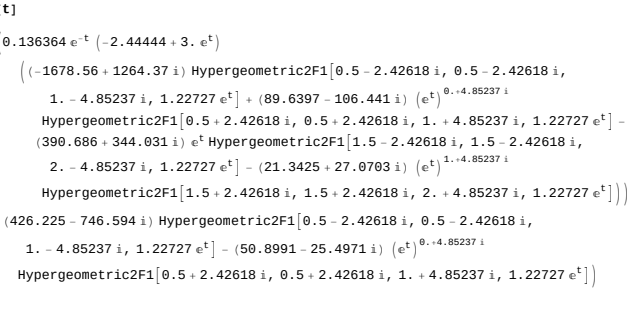

Fig. 5. Screen-shot of the the closed form solution for $Q(t)$ in (20) generated by *Mathematica* when numerical values are given to each variable (*e.g.*, $\epsilon_1 = 2.2\epsilon_0,\ \sigma_1 = 10^{-12}$ S/m, $\rho_e = -10^3$ C/m^3, $\mu_e = 10^{-4}$ m^2/V·s, $\epsilon_2 = \epsilon_0,\ \sigma_2 = 0.01$ S/m, $\tau_r = 4.78 \times 10^{-9}$ s, $\Upsilon_c = -0.222,\ \Sigma_c = 1,\ \tau_{pc} = 7.79 \times 10^{-10}$ s). The length and complexity of the solution is greatly reduced compared with the general solution shown partially in Fig. 4.

($\sigma_2 = 0.01$ S/m) to a poor conductor ($\sigma_2 = 1$ S/m)). The three permittivity values were chosen as most materials, such as Fe_3O_4, ZnO and Al_2O_3, have permittivities that range between ϵ_0 and $100\epsilon_0$. Note, the values used for E_0, ρ_e, μ_e, R, ϵ_1, and σ_1 in Fig. 6 were the same as given in Section IIIA.

The most striking feature of the results of Fig. 6 is the fact that there appears to be an upper limit to the rate at which a particle in transformer oil will charge and that this limit appears to be linked to the particle's conductivity, with upper limit being the perfect conductor case. A second interesting feature is that the particle charging dynamics appear to be less sensitive to variations in particle permittivity. Interestingly, the insensitivity to variations in permittivity is particularly evident for particles whose conductivity is greater than 1 S/m. A feature of the results is the fact that for less conductive particles, the charging rate appears to be higher for particles with higher permittivity. This behavior is particularly obvious in Fig. 6(a), where the charging dynamics of a particle with a conductivity of 0.01 S/m are plotted.

To assess the efficiency of the nanoparticles trapping capability to impact the electrodynamics in the high field ionization zone of the streamer tip, an estimation of electron-ion separation is determined using representative values of streamers. In the case of transformer oil, an electric field level of $E_0 = 1 \times 10^8$ V/m and a length of $d = 10$ μm are typical for the ionization zone, while electron mobility $\mu_e = 1 \times 10^{-4}$ m^2/V $\cdot$ s is appropriate. Consequently, the electron velocity in the ionization zone is approximately $v_e = -\mu_e E_0 = -1 \times 10^4$ m/s and the corresponding time required to sweep the electrons out of the ionization zone is $t_e = d/|v_e| = 1 \times 10^{-9}$ s.

The charging dynamics of highly conductive particles (*i.e.,* those with a conductivity of greater than 1 S/m) plotted in Fig. 6(c) indicate that during the electron sweep out time t_e a nanoparticle in the ionization zone can capture approximately $Q(t = t_e) \approx 1 \times 10^{-18}$C or six electrons. Therefore, the charging rate of conductive nanoparticles in transformer oil is enough to ensure the capture or trapping of six free electrons per nanoparticle in the ionization zone. This result is significant as it indicates that conductive nanoparticles, such as magnetite particles, which have been used to manufacture transformer oil-based nanofluids as done by Segal [2], can indeed capture free charge carriers at a rate that is sufficient to result in the modification of the electrodynamic processes responsible for the development of streamers in transformer oil-based nanofluids.

IV. Model of Streamer Propagation in Transformer Oil-Based Nanofluids

O'Sullivan *et al.* showed that electric field dependent molecular ionization is the key mechanism for positive streamer development in transformer oil [4], [5]. By ionizing oil molecules into slow positive ions and fast electrons, an area of net positive space charge quickly develops because the highly mobile electrons are swept away to the positive electrode from the ionization zone leaving behind the low mobility positive ions. The net homocharge modifies the electric field

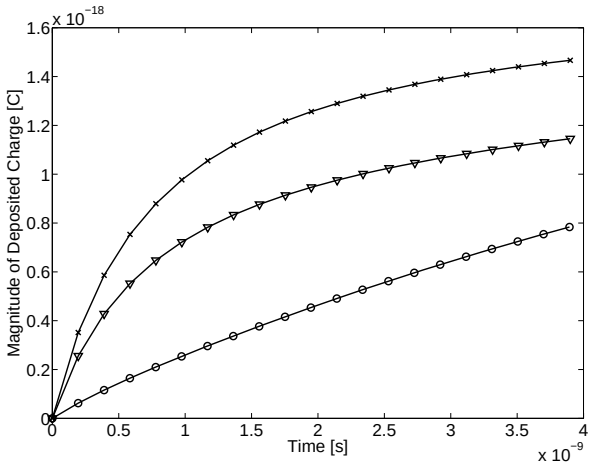

(a) $\sigma_2 = 0.01$ S/m

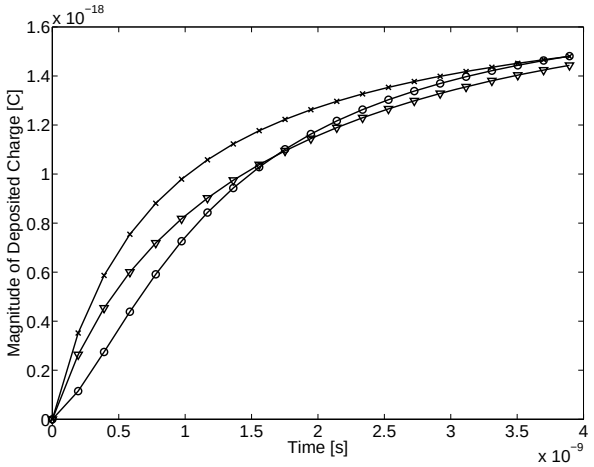

(b) $\sigma_2 = 0.1$ S/m

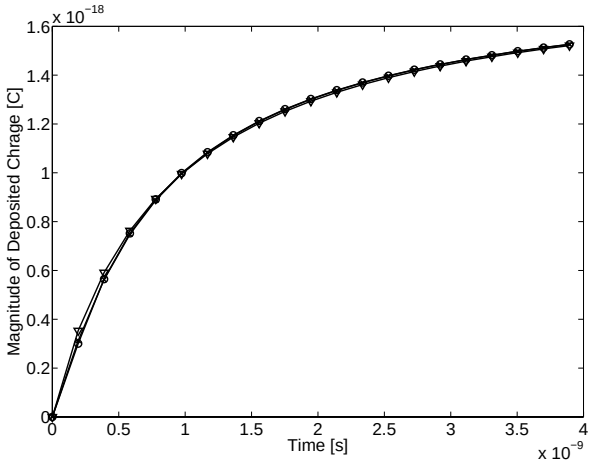

(c) $\sigma_2 = 1$ S/m

Fig. 6. Charging dynamics, $Q(t)$, of a nanoparticle with constant conductivity σ_2 and varying permittivity $\epsilon_2 = 1\epsilon_0(\bigcirc)$, $10\epsilon_0$ $(\bigtriangledown)$, and $100\epsilon_0$ $(\times)$ in transformer oil ($\sigma_1 = 1 \times 10^{-12}$ S/m, $\epsilon_1 = 2.2\epsilon_0$).

distribution in the oil such that the electric field at the positive electrode decreases while the electric field ahead of the positive charge in the oil increases. The new field distribution leads to ionization occurring further away from the positive electrode, which in turn causes further modification of the electric field distribution. The ultimate result of these electrodynamic processes is the development of an ionizing electric field wave, which is a moving dissipative source that raises the temperature to vaporize transformer oil and create a gas phase. This oil vaporization leads to the formation of the low density streamer channel in transformer oil.

Streamer propagation in a transformer oil-based nanofluid is still dependent on molecular ionization in the same manner as it is in pure oil. However, the dynamics that take place in the nanofluid subsequent to this differ from those in pure oil, depending upon the nanoparticle material's characteristics that determine the rate of nanoparticle charging. For a nanofluid manufactured using magnetite, the extremely short charging time of the nanoparticles, as shown by the analysis in Section III, indicate that they are excellent electron trapping particles. Therefore, the mobile electrons produced by ionization are trapped before they can be swept away from the ionization zone causing the electrodynamics involved in the development of an electric field wave in the nanofluid to be significantly modified from those in pure oil.

A. Governing Equations

The governing equations that contain the physics to model streamer development are based on the drift dominated charge continuity equations (36)-(39) for positive ion (ρ_p), negative ion (ρ_n), electron (ρ_e), and charged nanoparticle (ρ_{np}) densities which are coupled via Gauss' Law (35) and include the thermal diffusion equation (40) to model temperature rise in oil. The negative ion, electron, and charged nanoparticle densities are negative quantities.

$$\nabla \cdot (\epsilon \vec{E}) = \rho_p + \rho_n + \rho_e + \rho_{np} \tag{35}$$

$$\frac{\partial \rho_p}{\partial t} + \nabla \cdot (\rho_p \mu_p \vec{E}) = G_I + \frac{\rho_p \rho_e R_{pe}}{e} + \frac{\rho_p(\rho_n + \rho_{np}) R_{pn}}{e} \tag{36}$$

$$\frac{\partial \rho_n}{\partial t} - \nabla \cdot (\rho_n \mu_n \vec{E}) = \frac{\rho_e}{\tau_a} - \frac{\rho_p \rho_n R_{pn}}{e} \tag{37}$$

$$\frac{\partial \rho_e}{\partial t} - \nabla \cdot (\rho_e \mu_e \vec{E}) = -G_I - \frac{\rho_p \rho_e R_{pe}}{e} - \frac{\rho_e}{\tau_a} - \frac{\rho_e}{\tau_{np}}(1 - H(\rho_{np,sat} - \rho_{np})) \tag{38}$$

$$\frac{\partial \rho_{np}}{\partial t} - \nabla \cdot (\rho_{np} \mu_{np} \vec{E}) = \frac{\rho_e}{\tau_{np}}(1 - H(\rho_{np,sat} - \rho_{np})) - \frac{\rho_p \rho_{np} R_{pn}}{e} \tag{39}$$

$$\frac{\partial T}{\partial t} + \vec{v} \cdot \nabla T = \frac{1}{\rho_l c_v}(k_T \nabla^2 T + \vec{E} \cdot \vec{J}\,) \tag{40}$$

Parameters μ_p, μ_n, μ_e, and μ_{np} are the mobilities of the positive ions (1×10^{-9} m^2/V·s [11]), negative ions (1×10^{-9} m^2/V·s [11]), electrons (1×10^{-4} m^2/V·s [12], [13]) and charged nanoparticles (1×10^{-9} m^2/V·s), respectively. The

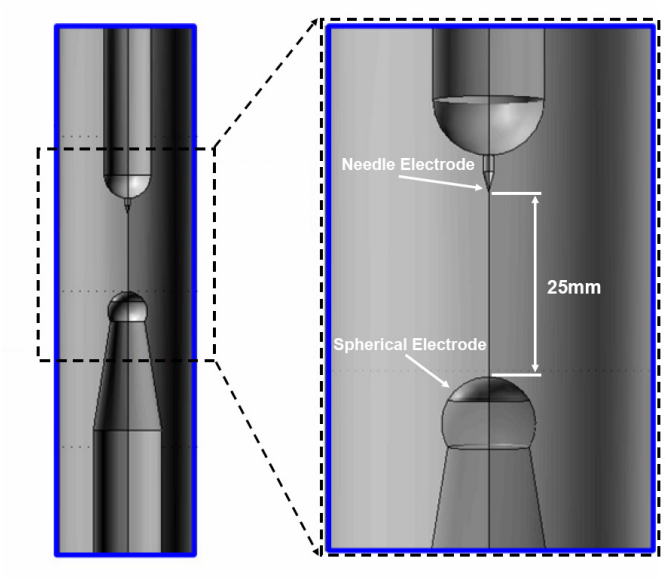

Fig. 7. Computer-aided design representation of the needle-sphere electrode geometry used for streamer simulation purposes.

electrodynamics are coupled to the oil's temperature through the $\vec{E} \cdot \vec{J}$ dissipation term in (40), where $\vec{J} = (\rho_p \mu_p - \rho_n \mu_n - \rho_e \mu_e - \rho_{np} \mu_{np})\vec{E}$ is the total current density. This term reflects the electrical power dissipation or Joule heating that takes place in the oil as a result of the motion of free charge carriers under the influence of the local electric field. Parameters $\vec{v}$, ϵ, k_T, c_v, and ρ_l are the oil's velocity, permittivity ($2.2\epsilon_0$), thermal conductivity (0.13 W/m·K), specific heat (1.7×10^3 J/kg·K), and mass density (880 kg/m^3), respectively, and these values are representative for transformer oil.

The boundary conditions applied to the streamer model of (35)-(40) are:

- Gauss' Law (35): The sharp needle and large diameter sphere electrodes are set to a 300 kV step voltage at $t = 0$ and 0 V, respectively. The symmetry z-axis and the top, bottom and side insulating walls have the boundary condition of zero normal electric field components (*i.e.*, $\vec{n} \cdot \vec{E} = 0$).
- Charge Transport Continuity Equations (36)-(39): The electrode boundary conditions along the outer insulating boundaries are $-\vec{n} \cdot \vec{J} = 0$. In addition, the necessary boundary condition at the electrodes is $\vec{n} \cdot \nabla \rho = 0$ because of the use of artificial diffusion to aid numerical convergence.
- Thermal Equation (40): All boundaries are set to zero inward normal thermal diffusive flux (*i.e.*, $\vec{n} \cdot (-k_T \nabla T) = 0$) making the approximation that the system is adiabatic on the timescales of interest.

The mathematical model described by the set of equations above is solved numerically using the finite element method software package COMSOL Multiphysics. The setup corresponds to the needle-sphere electrode geometry as shown in Fig. 7 and detailed in the IEC 60897 standard [24]. The axial distance between the needle electrode's tip and the spherical electrode is 25 mm. The radius of curvature of the needle electrode and spherical electrode are 40 μm and 6.35 mm,

respectively. The applied voltage to the needle electrode was a step voltage with a rise time of 0.01 μs and amplitude of 300 kV. The setup of the numerical model was in agreement with O'Sullivan *et al.* [4], [5] and the electrothermal model (35)-(40) are solved in their two dimensional form with azimuthal symmetry.

B. Electron Mobility

Transformer oil is not a pure liquid hydrocarbon, but is a mixture of many different naphthenic, paraffinic, and aromatic molecules with a complex molecular structure. It is this feature of transformer oil that makes it difficult to characterize many parameters such as electron mobility. The electron mobility in transformer oil, to the authors' best knowledge, has not been characterized. This is partially due to the reason stated above, as well as the varying sources, types and distributors of transformer oil. In this work, an educated estimate has been made on the electron mobility in transformer oil based upon the logarithmic average of the electron mobility of common saturated hydrocarbons. The electron velocity in these liquids range from 1×10^{-6} m^2/V·s to 1×10^{-2} m^2/V·s [12], [13]. Therefore, the electron velocity in transformer oil was chosen as 1×10^{-4} m^2/V·s in this work.

A method to validate this choice for electron mobility in transformer oil is via the classical electron radius, known as the Lorentz radius [6]. The electron is modeled as a small uniformly charged spherical volume of radius R_e with total charge $q = 4\pi R_e^3 \rho_0/3$. Tthe total work needed to assemble the electron sphere is [6]

$$W = \frac{3q^2}{20\pi\epsilon_0 R_e}. \tag{41}$$

Einstein's theory of relativity tells us that that this work necessary to assemble the charge is stored as energy that is related to the mass as $W = m_e c^2$ where c is the speed of light in free space. Equating the two expressions results in an expression for the electron radius as

$$R_e = \frac{3q^2}{20\pi\epsilon_0 m_e c^2}. \tag{42}$$

For the case of an electron ($q = -e = -1.6 \times 10^{-19}$ C, $m_e = 9.1 \times 10^{-31}$ kg) in free space, the radius is $R_e = 1.69 \times 10^{-15}$ m. Now using Walden's rule the electron mobility is

$$\mu_e = \frac{e}{6\pi\eta R_e} = 2.5 \times 10^{-4} \text{ m}^2/\text{V·s} \tag{43}$$

where $\eta = 0.02$ Pa/s is a representative value for the viscosity of transformer oil. This result, based on classical methods, is close to the selected electron mobility, thereby confirming that the selection of $\mu_e = 1 \times 10^{-4}$ m^2/V·s is reasonable.

C. Recombination and Electron Attachment

The Langevin-Debye relationship is used to model ion-ion and ion-nanoparticle recombination rates R_{pn} and ion-electron recombination rate R_{pe} in the transformer oil [11], [15], [16]. According to the Langevin-Debye relationship, the two recombination rates can be expressed as

$$R_{pn} = \frac{e(\mu_p + \mu_n)}{\epsilon} \tag{44}$$

$$R_{pe} = \frac{e(\mu_p + \mu_e)}{\epsilon}. \tag{45}$$

The ion-electron recombination rate of (45) is overestimated because these recombination relationships are diffusion limited and are valid for situations where the electric field levels are low to moderate and the recombining species are of similar physical scale [16]. It has been shown that the Langevin-Debye recombination model overestimates the rate of ion-electron recombination in liquids at low to moderate electric field levels [17], [18]. To compensate for the reduction in the recombination cross-section caused by high electric field levels, some authors have used the Langevin-Debye recombination term for ion-ion recombination to model ion/electron recombination [19]. This approach effectively compensates for the reduction in the recombination cross-section by reducing the apparent electron mobility. Using the respective value for each variable (*i.e.*, ion mobilities) the recombination rates are $R_{pn} = R_{pe} = 1.64 \times 10^{-17}$ m^3/s. In addition to recombination, electrons also combine with neutral molecules to form negative ions. This process is modeled as an electron attachment time constant, $\tau_a = 200$ ns [4], [19].

D. Charge Generation via Field Ionization

The field ionization charge density rate source term, G_I, was modeled using the Zener model of electron tunneling in solids [4], [5], [20], [21].

$$G_I(|\vec{E}|) = \frac{e^2 n_0 a |\vec{E}|}{h} \exp\left(-\frac{\pi^2 m^* a \Delta^2}{e h^2 |\vec{E}|}\right) \tag{46}$$

Parameter e is the electronic charge, a is the molecular separation distance (3×10^{-10} m [19]), $\vec{E}$ is the electric field, h is Planck's constant, m^* is the effective electron mass in the liquid ($0.1 \times m_e = 9.1 \times 10^{-32}$ kg), n_0 is the number density of ionizable species (1×10^{21} m^{-3} [22]) and Δ is the molecular ionization energy (1.136×10^{-18} J (7.1 eV) [23]). The values used for these parameters are consistent with those used by O'Sullivan *et al.* [4], [5].

E. Modeling Nanoparticle Charging

The analytical solution for the charging dynamics of a perfectly conducting nanoparticle in a transformer oil-based nanofluid is given by (13). In practical terms, modeling the charging dynamics of the nanoparticles is approximated by an attachment time constant τ_{np}. As the electrons are captured by the nanoparticles they are converted into slowly moving negatively charged carriers.

When including nanoparticle charging in the electrodynamic model, it is necessary to account for the fact that there is an upper limit to the charge density of free electrons which will be trapped by the nanoparticles. The nanoparticle charge density limit is $\rho_{np,sat} = n_{np} Q_s$, where n_{np} is the number density of nanoparticles. In (38) and (39) the Heaviside function, $H(\rho_{np,sat} - \rho_{np})$, is used to model this charging limit

$$H(\rho_{np,sat} - \rho_{np}) = \begin{cases} 0 & |\rho_{np}| < |\rho_{np,sat}| \\ 1 & |\rho_{np}| > |\rho_{np,sat}| \end{cases} \tag{47}$$

Note, both ρ_{np} and $\rho_{np,sat}$ are negative quantities. The selection of the time constant τ_{np} is done by referring to Fig. 3 and choosing the rise time value which is approximately 2 ns. A reasonable value of $\rho_{np,sat} = -500$ C/m^3 was chosen which correlates to a nanoparticle number density of $n_{np} \approx 2.7 \times 10^{20}$ m^{-3} with $Q_s = -1.836 \times 10^{-18}$ C.

It is important that the value of $\rho_{np,sat}$ that is used when modeling the electrodynamics in oil-based nanofluids be reasonable in order for the subsequent analysis to be valid. This value is derived from the nanoparticle charging analysis discussed in Section III along with certain assumptions regarding the composition of the transformer oil-based nanofluid. Assuming the magnetite nanoparticles have a radius $R = 5$ nm and the nanofluid has a saturation magnetization $\mu_0 M_s = 10^{-4}$ T or 1 Gauss, where $\mu_0 = 4\pi \times 10^{-7}$ H/m, the magnetite volume is $V_{np} = 4\pi R^3/3$ and the volume fraction ϕ of magnetite nanoparticles in the nanofluid is

$$\phi = \frac{M_s}{M_d} = 1.79 \times 10^{-4} \tag{48}$$

where the domain magnetization $\mu_0 M_d$ of magnetite is 0.56 T [25]. The nanoparticle charge density upper limit for trapping electrons $\rho^{\infty}_{np,sat}$ is then

$$\rho^{\infty}_{np,sat} = 11 \text{ electrons} \times \frac{-e}{V_{np}/\phi} = -600 \text{ C/m}^3 \tag{49}$$

but this assumes that the charging time is infinite. From Fig. 3, the perfectly conducting nanoparticle has charged to slightly under 80% of its total charge by $\tau_{np} = 2$ ns. Therefore, $\rho_{np,sat}$ is reduced from $\rho^{\infty}_{np,sat}$ and is chosen to be -500 C/m^3 corresponding to $\phi = 1.5 \times 10^{-4}$ to model the finite charging time of highly conductive nanoparticles such as magnetite.

V. Results and Discussion

The electric field dependent molecular ionization model is modified for use in modeling the dynamics in oil-based nanofluids by adding an extra term to both the electron and negative ion charge continuity equations. This term models the trapping of free electrons onto the nanoparticles in the nanofluid. Because of the presence of this additional term in the electron and negative ion charge continuity equations, it is reasonable to assume that the charge density distributions given by the solutions of the nanofluid molecular ionization model case study should differ from those given by the solution of the molecular ionization model for pure oil. Fig. 8 plots positive ion, negative ion, negatively charged nanoparticle, and electron charge density distributions along the needle-sphere electrode axis given by the solutions of the magnetite nanofluid molecular ionization model and the equivalent pure oil molecular ionization model at 0.1 μs after a 300 kV step voltage is applied. These plots highlight the differences between the charge density dynamics in nanofluids and those in pure oil.

In particular, Fig. 8(a) illustrates the effective electron trapping characteristic of the conductive nanoparticles. The magnitude of the pure oil negative ion charge density distribution in Fig. 8(b) increases smoothly from the ionization zone towards the needle electrode tip as free electrons are trapped on neutral molecules. The situation is very different for the nanofluid where the magnitude of the negative ion density rises rapidly at first, thereby significantly decreasing the electron density. Afterwards, the magnitude of the negative ion density transitions to a more gradual increase after the nanofluid charge density saturation ($\rho_{np,sat} = -500$ C/m^3) is reached. Due to the extremely fast trapping of the fast electrons by the low mobility nanoparticles the development of a net space charge zone at the streamer tip is hindered, suppressing the propagating electric field wave that is needed to continue electric field dependent molecular ionization. This behavior results in a major reduction in the velocity of the electric field wave as seen by the decrease in propagation distance from the needle electrode in Fig. 9(a) of the net space charge density in the nanofluid compared to pure oil.

To facilitate a direct comparison of streamer propagation in magnetite nanofluid and pure oil, the electric field distributions along the needle-sphere electrode axis at 0.1 μs are plotted in Fig. 9(b). The velocity of the electric field wave generated by the nanofluid model case study after 0.1 μs is about 45% slower than the velocity of the electric field wave generated by the equivalent model for molecular ionization in pure oil [5]. This result is extremely significant as it confirms that the presence of conductive nanoparticles in transformer oil would reduce the velocity of the electric field wave generated by molecular ionization in the liquid and thereby decrease streamer velocity. The model gives a 64% average positive streamer velocity decrease from 1.65 km/s in pure transformer oil to 1.05 km/s in the nanofluid. These velocities are extremely close to the average velocities obtained by Segal *et al.* [2] that are summarized in Table I.

VI. Conclusion

This paper develops a theory to explain the differences observed between the electrical breakdown characteristics of transformer oil and transformer oil-based nanofluids. A general expression for the charging of nanoparticles in a dielectric liquid is presented and it is shown that the charging time constant τ_{pc} from (12) of conductive nanoparticles, such as magnetite, in transformer oil is over two orders of magnitude faster than the timescale involved in streamer development in transformer oil. Therefore, for the purposes of streamer analysis assuming infinite conductivity for conductive magnetite nanoparticles is justified.

Using the generalized analysis of the charging dynamics for finitely conducting nanoparticles, a complete electrodynamic model is developed. The simulation study shows that the significant dynamics in the electric field and thermal enhancement in highly electrically stressed nanofluid are due to molecular ionization just as in transformer oil. However, streamer propagation is hindered because the charging of slow conductive nanoparticles by electrons in the ionization zone changes fast electrons into slow negatively charged nanoparticles that modifies the electrodynamics in the oil and slows the propagation of positive streamers.

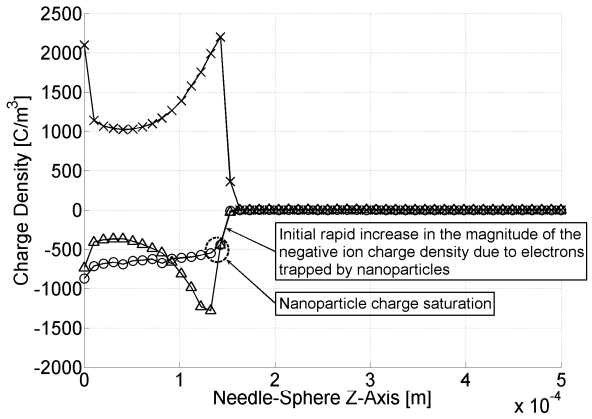

(a) Transformer Oil-Based Magnetite Nanofluid; Legend: ρ_p $(-\times-)$, $\rho_n + \rho_{np}$ $(-\bigcirc-)$, ρ_e $(-\triangle-)$.

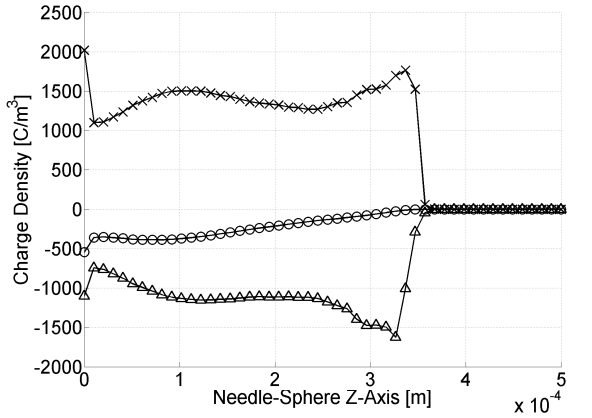

(b) Pure Transformer Oil; Legend: ρ_p $(-\times-)$, ρ_n $(-\bigcirc-)$, ρ_e $(-\triangle-)$.

Fig. 8. Charge density distributions along the needle-sphere electrode axis at time t $= 0.1$ μs given by the solution to the streamer model for transformer oil and transformer oil-based nanofluid with $\rho_{np,sat} = -500$ C/m^3 and $\tau_{np} = 2$ ns.

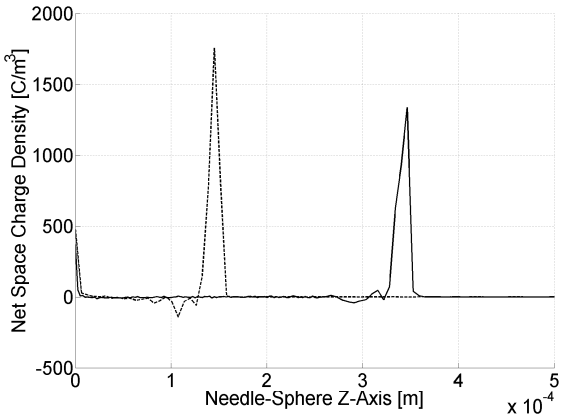

(a) Net Space Charge Density

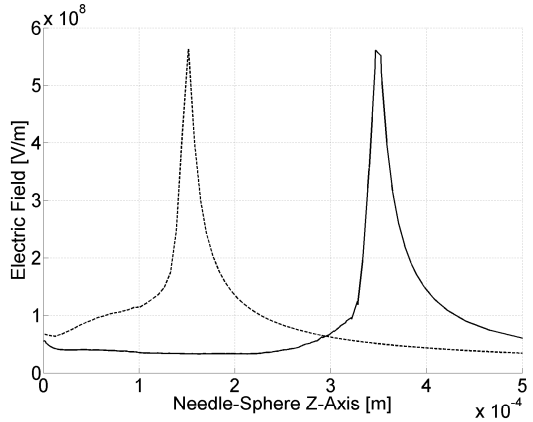

(b) Electric Field

Fig. 9. Net space charge density and electric field distributions along the needle-sphere electrode axis at time t $= 0.1$ μs given by the solution to the streamer model for transformer oil (—) and transformer oil-based nanofluid (- - -) with $\rho_{np,sat} = -500$ C/m^3 and $\tau_{np} = 2$ ns, clearly showing the decrease in streamer propagation velocity for the transformer oil-based nanofluid.

ACKNOWLEDGMENT

This work has been supported by ABB Corporate Research, Västerås, Sweden.

REFERENCES

[1] V. Segal and K. Raj, "An investigation of power transformer cooling with magnetic fluids," *Indian J. Eng. Mater. Sci.*, Vol. 5, No. 6, pp. 416-422, 1998.

[2] V. Segal, A. Hjortsberg, A. Rabinovich, D. Nattrass, and K. Raj, "AC(60Hz) and impulse breakdown strength of a colloidal fluid based on transformer oil and magnetite nanoparticles," in *IEEE International Symposium on Electrical Insulation ISEI98*, Arlington, VA, USA, June 7-10, 1998, pp. 619-622.

[3] V. Segal, A. Rabinovich, D. Nattrass, K. Raj, and A. Nunes, "Experimental study of magnetic colloidal fluids behavior in power transformers," *J. Magn. Magn. Mater.*, Vol. 215, pp. 513-515, 2000.

[4] F. M. O'Sullivan, "A model for the initiation and propagation of electrical streamers in transformer oil and transformer oil based nanofluids," Ph.D. dissertation, Massachusetts Institute of Technology, Cambridge, MA, USA, 2007.

[5] F. O'Sullivan, J. G. Hwang, M. Zahn, O. Hjortstam, L. Pettersson, R. Liu, and P. Biller, "A model for the initiation and propagation of positive streamers in transformer oil," in *Proc. IEEE International Symposium on Electrical Insulation ISEI08*, Vancouver, British Columbia, Canada, June 2008, pp. 210-214.

[6] M. Zahn, *Electromagnetic Field Theory: A Problem Solving Approach*. Malabar: Robert E. Krieger Publishing Company, Inc., 2003, Chap. 3, 4.

[7] J. R. Melcher, *Continuum Electromechanics*. Cambridge: The MIT Press, 1981, Section 5.1-5.5.

[8] J. M. D. Coey, A. E. Berkowitz, L. I. Balcells, F. F. Putris and F. T. Parker, "Magnetoresistance of magnetite," *Appl. Phys. Letts.,* Vol. 72, No. 6, pp. 734-736, 1998.

[9] A. Dey, A. De and S. K. De, "Electrical transport and dielectric relaxation in Fe_3O_4-polypyrrole hybrid nanocomposites," *J. Phys.: Condens. Matter.*, Vol. 17, pp. 5895-5910, 2005.

[10] F. J. W. Whipple and J. A. Chalmers, "On Wilson's theory of the collection of charge by falling drops," *Quart. J. Roy. Met. Soc.,* Vol. 70, p. 103, 1944.

[11] U. Gäfvert, A. Jaksts, C. Törnkvist and L. Walfridsson, "Electrical field distribution in transformer oil," *IEEE Trans. Electr. Insul.*, Vol. 27, No. 3, pp. 647-660, June 1992.

[12] W. F. Schmidt, "Electronic conduction processes in dielectric liquids," *IEEE Trans. Electr. Insul.*, Vol. EI-19, No. 5, pp. 389-418, October 1984.

[13] A. O. Allen, *Drift Mobilities and Conduction Band Energies of Excess Electrons in Dielectric Liquids*, NSRDS-NBS: Washinton, 1976.

[14] S. Wolfram, *The Mathematica Book*, 4^{th} ed. Cambridge: Wolfram Media/Cambridge University Press, 1999.

[15] A. Denat, B. Gosse and J. P. Gosse, "Electrical conduction of solutions of an ionic surfactant in hydrocarbons," in *Proc. International Conference on Dielectric Liquids*, Berlin, Germany, July 1981, pp. 130-134.

[16] W. F. Schmidt, *Liquid State Electronics of Insulating Liquids*. Boca Raton: CRC Press, 1997.

[17] Y. Nakamura, K. Shinsaka and Y. Hatano, "Electron mobilities and electron-ion recombination rate constants in solid, liquid and gaseous methane," *J. Chem. Phys.*, Vol. 78, No. 9, pp. 5820-5824, 1983.
[18] M. Tachiya, "Breakdown of the Debye theory of bulk ion recombination," *J. Chem. Phys.*, Vol. 87, No. 7, pp. 4108-4113, 1987.
[19] J. Qian, R. P. Joshi, E. Schamiloglu, J. Gaudet, J. R. Woodworth, and J. Lehr, "Analysis of polarity effects in the electrical breakdown of liquids," *J. Phys. D: Appl. Phys.,* Vol. 39, pp. 359-369, 2006.
[20] C. Zener, "A theory of the electrical breakdown of solid dielectrics," *Proc. Roy. Soc. A,* Vol. 145, No. 855, pp. 523-529, 1934.
[21] J. C. Devins, S. J. Rzad and R. J. Schwabe, "Breakdown and prebreakdown phenomena in liquids," *J. Appl. Phys.,* Vol. 52, No. 7, pp. 4531-4545, July 1981.
[22] W. G. Chadband, "On variations in the propagation of positive discharges between transformer oil and silicone fluids," *J. Phys. D: Appl. Phys.,* Vol. 13, pp. 1299-307, 1980.
[23] M. Harada, Y. Ohga, I. Watanabe, and H. Watarai, "Ionization energies for solvated polycyclic aromatic hydrocarbons," *Chem. Phys. Lett.*, Vol. 303, pp. 489-492, 1999.
[24] IEC Standard #60897, "Methods for the determination of the lightning impulse breakdown voltage of insulating liquids."
[25] R. E. Rosensweig, *Ferrohydrodynamics*. New York: Dover Publications, 1997.

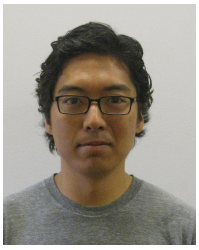

J. George Hwang received the B.A.Sc. and M.A.Sc. degrees in electrical engineering from the University of Toronto, Toronto, ON, Canada in 2004 and 2007, respectively. He is currently pursuing a Ph.D. at the Massachusetts Institute of Technology, Cambridge, MA, USA.

From 2005 to 2006, he was with the Power Electronic Systems Group, ABB Switzerland Ltd Corporate Research Center, Baden, Switzerland. Prior to that he was with the Systems Integration Group, Hydrogenics Corporation, Mississauga, ON Canada working on fuel cell power systems.

Markus Zahn received the Sc.D. degree in 1970 from the Department of Electrical Engineering at the Massachusetts Institute of Technology; then joined the Department of Electrical Engineering at the University of Florida, Gainesville until 1980 when he returned to MIT where he is now the Thomas and Gerd Perkins Professor of Electrical Engineering working in the Laboratory for Electromagnetic and Electronic Systems and the MIT High Voltage Research Laboratory. He is also the Director of the MIT EECS Course VI-A Internship Program, a cooperative work/study program with industry. His primary current research areas are ferrohydrodynamics and electrohydrodynamics for microfluidic, biomedical, and micro/nanoelectromechanical system (MEMS/NEMS) applications; nanoparticle technology for improved high voltage performance of electric power apparatus; Kerr electrooptic field and space charge mapping measurements in high voltage stressed materials; and model based interdigital dielectrometry and magnetometry sensors for non-destructive testing and evaluation applications and for identification of metallic and non-metallic land mines and unexploded ordnance. Professor Zahn is co-inventor on 19 patents; has written the textbook Electromagnetic Field Theory: A Problem Solving Approach; about 10 book and encyclopedia chapters; about 115 journal publications and about 175 conference papers; and has co-produced a set of educational videotapes for the enriched teaching of electromagnetism. He is a Fellow of the IEEE; was a Distinguished Visiting Fellow of the Royal Academy of Engineering at the University of Manchester, England; is an Associate Editor of the IEEE Transactions on Dielectrics and Electrical Insulation; and is on the International Scientific Committee on Magnetic Fluids.

Francis M. O'Sullivan received the Ph.D., E.E. and S.M. degrees in 2007, 2006 and 2004 respectively from the Department of Electrical Engineering and Computer Science at the Massachusetts Institute of Technology. He received the B.E. degree from the Department of Electrical Engineering at the National University of Ireland - University College Cork in 2002. He is currently a Postdoctoral Associate with the Massachusetts Institute of Technology Energy Initiative. From 2007 to 2009, he worked as an Associate with the energy practice of the management consultancy group, McKinsey & Company. From 2004 to 2005, he worked as an engineering consultant with Exponent/Failure Analysis Associates, Natick MA.

Leif A. A. Pettersson received the Ph.D. degree in 1999 from the Department of Physics and Measurement Technology at Linköping University in Sweden. He received the B.Sc. in Computer Technology and Electronics in 1991 and the M.Sc. in Applied Physics and Electrical Engineering in 1995 from the same University. He joined ABB Corporate Research in 2001 and has since then been active in nanotechnology related research at the company especially within the field of insulating liquids and liquid impregnated solid insulation for power transformers. He is co-inventor on a number of patents as well as author and co-author of more than 30 journal publications and conference papers. Dr. Pettersson is at present Group Manager at ABB's Research Centre in Västerås.

Olof Hjortstam received the M.A.Sc. degree in physical engineering and a Ph.D degree in theoretical solid state physics from the University of Uppsala, Sweden in 1993 and 1997, respectively. Since 1998 he has be with ABB in Västerås, Sweden and has been active in a large variety of fields such as semiconductor physics, material physics, high voltage engineering, electromagnetism, breakdown physics in electrical insulation, and electro technical applications in process metallurgy.

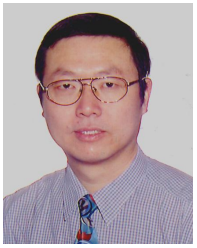

Rongsheng Liu received the Ph.D. degree in 1988 from the Department of Electrical Engineering at the Xi'an Jiaotong University in China, and did his post-doctoral work at the Electronic Measurement Laboratory at the Musashi Institute of Technology in Tokyo from July 1990 through June 1992. He then joined ABB Corporate Research in Sweden in July 1992 and has since been working there in the area of power technologies. His fields of research and interest encompass dielectrics and electrical insulation especially in power transformers and power cables. He is an inventor on 18 patents, and has been an author or co-author of 110 technical publications and reports. He is a winner of 3 technical awards and is a Senior Member of the IEEE. He has been an Associate Professor at the State Key Laboratory of Electrical Insulation and Power Equipment at the Xi'an Jiaotong University during the time he was in China since 1990.